

TEXTURES AND REVERSIBLE WATERMARKING

Ioan-Catalin Dragoi, Dinu Coltuc

Electrical Engineering Dept.,
Valahia University of Targoviste, Romania
email: {dragoi,coltuc}@valahia.ro

ABSTRACT

This paper investigates the effectiveness of prediction-error expansion reversible watermarking on textured images. Five well performing reversible watermarking schemes are considered, namely the schemes based on the rhombus average, the adaptive rhombus predictor, the full context predictor as a weighted average between the rhombus and the four diagonal neighbors, the global least-squares predictor and its recently proposed local counterpart. The textured images are analyzed and the optimal prediction scheme for each texture type is determined. The local least-squares prediction based scheme provides the best overall results.

Index Terms— reversible watermarking, textures, adaptive prediction, least square predictors

1. INTRODUCTION

For classical watermarking, the images with high content of textures provide more capacity for data hiding than the one without textures. This is due to the fact that the human visual system is less sensitive to degradation in textured areas and thus one can embed more in textured than in uniform areas (see [1], etc.). For reversible watermarking, this is not true: one can embed more data in uniform than in textured areas. This can be easily explained by the fact that the reversible watermarking schemes are based on pixel correlation, and the correlation in textured areas is lower than in uniform areas.

We remind that reversible watermarking not only demands imperceptible embedding of data, but also the recovery of the original host without any errors. The algorithms providing the highest embedding bit-rates are the so called difference expansion reversible watermarking [2, 3], etc. Difference expansion creates room for data embedding into the least significant bit (LSB) of a certain pixel based difference, usually into the prediction error. More precisely, pixels are modified such that, the prediction error at detection be two times larger. The multiplication by two sets to zero the LSB and leaves room for a bit of data. Obviously, the distortion

introduced by embedding one bit into a pixel is directly connected to the difference to be expanded. Otherwise stated, for prediction error expansion schemes, the performance depends on the prediction.

While the results of reversible watermarking are usually provided for images with different statistics, no analysis has been dedicated to textures. It should be noticed that a high content of texture exists in remote sensing images, medical images, etc.

This paper investigates the effectiveness of reversible watermarking for textured images. We focus on the performances of prediction error expansion reversible watermarking schemes. Five schemes are considered, namely the one based on the average on the rhombus context [5], the context adaptive rhombus of [6], the full context of [7], the global least-squares predictor and the local predictor very recently proposed in [8]. The global and local prediction schemes are using the rhombus context as well. In fact, it should be noticed that most of the recently proposed schemes are using the rhombus context (see [6]- [12]). The results are evaluated on the well-known Brodatz album. The outline of the paper is as follows. The basic principle of the reversible watermarking based on prediction error expansion and the particularities of the selected schemes are briefly presented in Section 2. Experimental results are provided in Section 3. In Section 4, the conclusions are drawn.

2. PREDICTION ERROR EXPANSION SCHEMES

The basic principle of prediction error expansion reversible watermarking is first introduced. Then, the selected schemes are briefly discussed.

2.1. Basic Principle

An integer threshold (T) is defined in order to control the distortion and implicitly, the embedding bit-rate of the watermarking scheme. For each pixel, the prediction error is computed,

$$e_{i,j} = x_{i,j} - \hat{x}_{i,j} \quad (1)$$

where $\hat{x}_{i,j}$ is the predicted value of $x_{i,j}$. The pixels with $-T \leq e_{i,j} < T$ are used for embedding a bit of data ($b_{i,j}$),

This work is supported by the Romanian National Authority for Scientific Research, UEFISCDI, projects PN-II-PT-PCCA-2011-3.2-1162 and PN-II-PT-PCCA-2013-4-1762.

while the others are shifted in order to provide, at detection, a prediction error greater than the embedded pixels. Thus, one has:

$$x'_{i,j} = \begin{cases} x_{i,j} + e_{i,j} + b_{i,j} & \text{if } -T \leq e_{i,j} < T, \\ x_{i,j} + T & \text{if } e_{i,j} \geq T, \\ x_{i,j} - T + 1 & \text{if } e_{i,j} < -T. \end{cases} \quad (2)$$

Both the embedding and the shifting are possible if no overflow or underflow is generated, i.e., $0 \leq x'_{i,j} \leq 255$.

The performance of the prediction error expansion reversible watermarking depends on the prediction scheme. Next, we briefly present the five schemes considered in this paper.

2.2. Rhombus average

The use of the average on the rhombus context for prediction in reversible watermarking was introduced in [5]. This scheme starts by splitting the image into two sets, diagonally connected (like the black and white squares of a chessboard): the cross set and the dot set. The embedding starts with the pixels from the cross set and continues with the dot set only after all the pixels from the cross set were processed. The predicted value is computed as :

$$\hat{x}_{i,j} = \left\lfloor \frac{x_{i-1,j} + x_{i+1,j} + x_{i,j-1} + x_{i,j+1}}{4} \right\rfloor \quad (3)$$

The pixels of the cross set are predicted by using only original pixels, i.e., the ones of the dot set. On the other hand, the pixels in the dot set are predicted by using modified pixels. This two-stages scheme appears to slightly outperform the simple raster scan watermarking where pixels are predicted by using two original and two modified pixels into the prediction context.

The two-stages approach allows a very fine control of the embedding bit-rate. More precisely, the pixels of each set are ordered according to the variance of their context:

$$\mu_{i,j} = \frac{1}{4} \sum_{k=1}^4 (\Delta\nu_k - \Delta\bar{\nu})^2 \quad (4)$$

where $\Delta\nu_1 = |x_{i,j-1} - x_{i-1,j}|$, $\Delta\nu_2 = |x_{i-1,j} - x_{i,j+1}|$, $\Delta\nu_3 = |x_{i,j+1} - x_{i+1,j}|$, $\Delta\nu_4 = |x_{i+1,j} - x_{i,j-1}|$ and $\Delta\bar{\nu} = (\Delta\nu_1 + \Delta\nu_2 + \Delta\nu_3 + \Delta\nu_4)/4$. Only the first n pixels with the smallest variance values from each set are considered for embedding, the remaining pixels are left unchanged. Not only very fine control of the embedding capacity is ensured, but also the number of shifted pixels is reduced [5].

2.3. Adaptive rhombus

The context adaptive rhombus of [6] selects one of three sub-predictors based on the local gradients (horizontal line, verti-

cal line, uniform area). The predicted value is computed as:

$$\hat{x} = \begin{cases} \lfloor (x_{i,j-1} + x_{i,j+1})/2 \rfloor, & \text{if } d_h < d_v, D \geq T_u \\ \lfloor (x_{i-1,j} + x_{i+1,j})/2 \rfloor, & \text{if } d_h > d_v, D \geq T_u \\ \lfloor (x_{i-1,j} + x_{i+1,j} + x_{i,j-1} + x_{i,j+1})/4 \rfloor, & \text{otherwise} \end{cases} \quad (5)$$

where $d_h = |x_{i,j-1} - x_{i,j+1}|$, $d_v = |x_{i-1,j} - x_{i+1,j}|$ and $D = |x_{i,j-1} + x_{i,j+1} - x_{i-1,j} - x_{i+1,j}|/2$. A uniformity threshold, T_u , is used to determine the smoothness of the current context.

Just like in the previous scheme, the embedding is performed in two stages and variance based sorting can be used to fine tune the results.

2.4. Full 3×3 context

The scheme introduced in [7] extends the rhombus to the entire 3×3 window by considering the diagonal neighbors as well. The predicted value is computed as weighted average: 75% of the average of the horizontal/vertical neighbors and 25% of the average of the diagonal neighbors.

As in [5], the smoothness of the context is checked. In [7], instead of variance, the difference between the maximum and the minimum graylevel on the prediction context is used. Obviously, the difference between the maximum and the minimum is less costly than the variance on the prediction context.

2.5. Global prediction

The global least-squares predictor computes weights for the neighbors in the selected context in order to minimize the sum of the squares of the prediction error. Let \mathbf{y} be the column vector obtained by scanning the entire image along the rows and let \mathbf{X} be the matrix whose rows are the corresponding context vectors of \mathbf{y} . The weights are computed as:

$$\mathbf{v} = (\mathbf{X}'\mathbf{X})^{-1}\mathbf{X}'\mathbf{y} \quad (6)$$

For the rhombus context, the predicted value of each pixel is computed as:

$$\hat{x}_{i,j} = \left\lfloor \sum_{k=1}^4 \mathbf{v}(k)x_{i,j}^k \right\rfloor \quad (7)$$

where $x_{i,j}^k$ are the four neighbors that form the rhombus context: $x_{i-1,j}$, $x_{i,j-1}$, $x_{i+1,j}$ and $x_{i,j+1}$.

\mathbf{X} can be extended by adding a first element, $x_{i,j}^0 = 1$, this allows equation (7) to also include a constant term:

$$\hat{x}_{i,j} = \left\lfloor \mathbf{v}(0) + \sum_{k=1}^4 \mathbf{v}(k)x_{i,j}^k \right\rfloor \quad (8)$$

The weights must be inserted in the payload as auxiliary data in order to make them available at the detection stage.

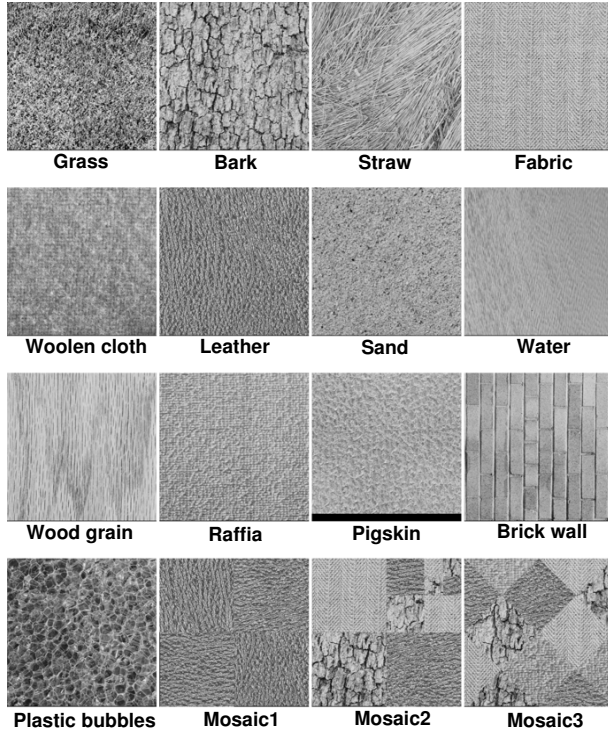


Fig. 1. The thirteen test images from the Brodatz set and the three mosaic images.

2.6. Local prediction

The local least-squares predictor of [8] computes a distinct predictor for each pixel. This approach uses a $B \times B$ block centered on the current pixel for determining the corresponding weights, instead of the entire image. The current pixel is replaced in the $B \times B$ block with an estimated value computed with (3) in order to make the block available at detection. This removes the need to transmit the weights to the decoder, they can be recomputed with (6) from the corresponding block. For this scheme a raster scan order is used for embedding and reverse raster scan order for decoding.

Equation (8) outperforms (7) for local prediction (they offer similar results for global prediction). Local prediction is a more computational approach than the global prediction, The total cost of computing a distinct predictor for each pixel is B^2 greater than using a single global predictor.

3. EXPERIMENTAL RESULTS

In this section, experimental results on textured images for the five reversible watermarking schemes of Section 2 are presented. Thirteen 512×512 graylevel images from the Brodatz set are used. The thirteen test images are presented in Fig.1 together with three additional mosaic images used to

test the stability of the global predictor with respect to the other schemes.

Before going any further, let us first discuss the performances of the selected schemes on the classical test images commonly used reversible watermarking (*Lena*, *Mandrill*, *Jetplane*, etc.). Both the adaptive rhombus scheme of [6] and the full context prediction of [7] offer slightly better results than the rhombus average based scheme of [5]. The adaptive rhombus tends to perform better on images with well defined contour lines and good contrast, but brings negligible improvements over the rhombus average on images with large uniform areas. Meanwhile, the full context predictor tends to have better results on these uniform images, but a stronger local variation can be a problem for the larger prediction context. The global least-squares predictor is more dependent on the host image and while it can outperform the rhombus average, statistically it offers similar results. The local least-squares predictor introduced in [8] clearly outperforms the other schemes, mainly on images with well defined contour lines. For both the global and local least-squares predictors the rhombus context is used, which was shown to have the best results in [8].

The local predictor remains the most reliable of the five schemes on the thirteen test images from the Brodatz set. The average and maximum gain in PSNR offered by the local prediction scheme with respect to the other four watermarking schemes are presented in Table 1. The results are obtained for 12×12 pixel blocks, size that remains statistically optimal for this set. By using the ideal size of the block for each image brings an average gain of only 0.16 dB on the entire set.

The full context scheme of [7] was outperformed by the other four approaches on all test images. The larger variation between neighboring pixels, caused by the textures, disrupted the already slightly weaker prediction offered by the diagonal neighbors, which in turn hampered the overall prediction on the eight pixel context.

The rhombus average based scheme of [5] outperformed the full context approach with an average gain in PSNR of 0.73 dB for the entire thirteen image set. The adaptive rhombus of [6] offers an average gain of 0.62 dB over the rhombus average. The largest average gain on a single image is 3.22 dB for the *Wood grain* texture. The large number of vertical lines of this texture proved problematic for both the rhombus average and the full eight pixel context predictors.

The adaptive rhombus was outperformed by the rhombus average on six test images: *Bark*, *Fabric*, *Woolen cloth*, *Sand*, *Pigskin* and *Brick wall*. The loss in PSNR is at most 0.68 dB (on *Woolen cloth*). The global least-square predictor obtained a gain in PSNR of 0.39 dB over the adaptive rhombus and had similar results with the ones offered by the local prediction on eight test images.

Based on the prediction results, the thirteen textured images can be split into three categories: chaotic, complex and stable. On chaotic textures (*Woolen cloth* and *Sand*) all the

Table 1. Gain in PSNR of the local prediction scheme with respect to the rhombus average of [5], the adaptive rhombus of [6], the full context of [7] and the global predictor on the textured images.

Test image	LP vs [5]		LP vs [6]		LP vs [7]		LP vs GP	
	Average [dB]	Maximum [dB]						
Grass	2.8	4.1	1.9	3.5	4.3	5.8	0.6	1.3
Bark	0.81	1.8	1.2	1.8	1.7	3	0.17	0.44
Straw	3.8	5.7	1.7	2.3	4.3	6.7	2.9	4.2
Fabric	0.97	2.9	1.3	1.7	2	4.9	-0.14	0
Woolen cloth	0	0.23	0.69	1.3	0.3	2.3	-0.04	0.06
Leather	1.8	2.8	0.38	1.4	2.6	3.8	0.02	0.73
Sand	0.06	0.4	0.39	0.99	0.57	1.4	-0.09	0.12
Water	1.3	1.9	1.1	1.4	2.4	3.5	1.1	1.4
Wood grain	4.8	5.2	1.5	4	5.7	7.2	0.25	0.43
Raffia	1.2	1.5	-0.4	1.8	2.5	2.9	0.18	0.45
Pigskin	0.79	2.7	1.2	2.7	1.1	3.8	0.54	3
Brick wall	0.45	0.88	0.61	1.3	0.75	2.3	0.11	0.31
Plastic bubbles	1.2	1.8	0.44	1.2	1.7	2.4	1.2	2
Average gains	1.5	2.5	0.94	2	2.3	3.8	0.53	1.1

predictors offer similar results. The distribution of graylevel values for the neighbors tends to vary from pixel to pixel, not just from region to region. For this type of textures the rhombus average, the less complex of the five predictors, is the most suitable approach. Complex textures (*Grass*, *Straw*, *Water* and *Plastic bubbles*), while varying from region to region, tend to have a clear local pattern. For these textures local prediction is ideal and brings considerable improvements over to other prediction schemes. And finally, stable textures (*Bark*, *Fabric*, *Leather*, *Wood grain*, *Raffia* and *Brick wall*) have a considerably reduced variation between regions relative to the other texture types. Because of this lack of variation, the use of local prediction does not bring any significant improvements over its global counterpart.

The global prediction has overall good results on the set, but its performance is mainly due to the texture stability of the host image. Thus, let us next consider a simple experiment. The test image *Leather* (which has a stable texture) is split into four equal sized regions, three regions are then rotated (the first by 90° , the second by 180° and the third by 270°) forming the *Mosaic1* image. The results of the five predictors on the new image are presented in Fig. 2. The variation between regions induced by rotation has caused an average drop in PSNR of 1.5 dB for the global predictor, while the effect on the other predictors is negligible.

An image can contain multiple textures. In order to simulate this case, we created the images *Mosaic2* and *Mosaic3* by combining parts of different textures. Notice that, the used textures (*Bark*, *Fabric*, *Leather* and *Rafia*) are all stable textures, the global and local predictors had similar results on them. Fig. 2 shows that for both mosaic images the global predictor has a drop in performance relative to the local pre-

dictor of 0.54 dB on *Mosaic2* and 0.48 dB on *Mosaic3*. For images with multiple textures the performance of all the tested watermarking schemes, except the global prediction, can be determined by evaluating the performance on each individual texture. Multiple textures are problematic for the global predictor especially when they have conflicting orientations.

4. CONCLUSIONS

The results of prediction error expansion reversible watermarking for texture images have been analyzed. Five prediction schemes defined on the rhombus context have been considered and the textures have been classified accordingly. As expected, the local least-squares based scheme provides very good results. On some textures, the global predictor based scheme can give almost similar results with the local predictor based ones.

REFERENCES

- [1] J. Huang and Y. Q. Shi, "Adaptive image watermarking scheme based on visual masking", *Electronics Letters*, vol. 34, no. 8, p. 748–750, 1998.
- [2] D. M. Thodi and J. J. Rodriguez, "Expansion Embedding Techniques for Reversible Watermarking", *IEEE Trans. Image Process.*, vol. 15, pp. 721–729, 2007.
- [3] Y. Hu, H.-K. Lee and J. Li, "DE-based reversible data hiding with improved overflow location map", *IEEE Trans. Circuits Syst. Video Technol.*, vol. 19, no. 2, pp. 250–260, 2009.

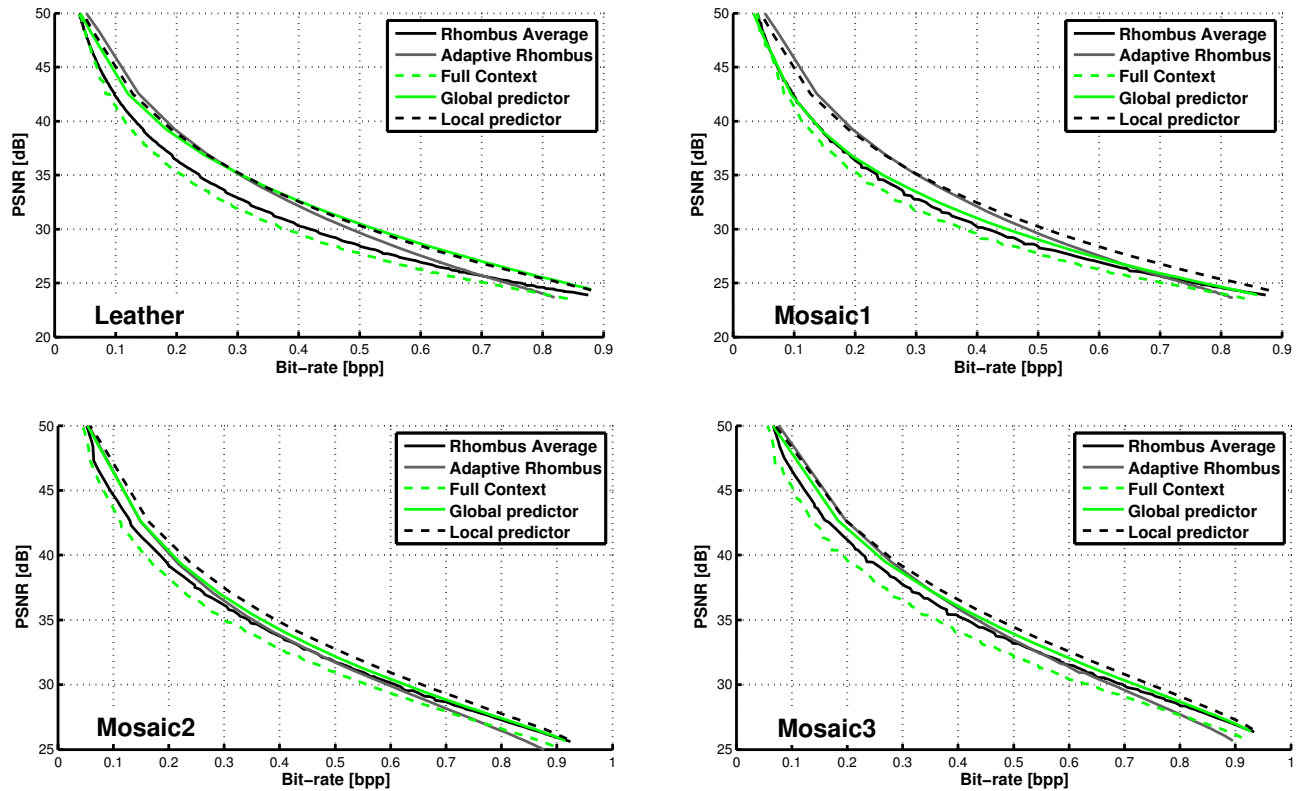


Fig. 2. Results of the five reversible watermarking schemes on the test image *Leather* and the three mosaic images.

[4] D. Coltuc, "Improved Embedding for Prediction Based Reversible Watermarking", *IEEE Trans. Inf. Forensics Security*, vol. 6, no. 3, 2011.

[5] V. Sachnev, H. J. Kim, J. Nam, S. Suresh and Y. Q. Shi, "Reversible Watermarking Algorithm Using Sorting and Prediction", *IEEE Trans. Circuits Syst. Video Technol.*, vol. 19, pp. 989–999, 2009.

[6] I.-C. Dragoi, D. Coltuc, "Improved Rhombus Interpolation for Reversible Watermarking by Difference Expansion", *Proc. 20th European Conf. on Signal. Process., EUSIPCO'2012*, pp. 1688–1692, 2012.

[7] X. Li, B. Li, B. Yang and T. Zeng, "General Framework to Histogram-Shifting-Based Reversible Data Hiding", *IEEE Trans. on Image Process.*, vol. 22, no. 6, pp. 2181–2191, 2013.

[8] I.-C. Dragoi and D. Coltuc, "Local Prediction Based Difference Expansion Reversible Watermarking", *IEEE Trans. on Image Process.*, DOI: 10.1109/TIP. 2014. 2307482, 2014.

[9] B. Ou, X. Li, Y. Zhao, and R. Ni, "Reversible data hiding based on PDE predictor", *Journal of Systems and Software*, vol. 86, no. 10, pp. 2700-2709, 2012.

[10] W. Zhang, X. Hu, X. Li, and N. Yu, "Recursive Histogram Modification: Establishing Equivalency between Reversible Data Hiding and Lossless Data Compression", *IEEE Trans. on Image Process.*, vol. 22, no. 7, pp. 2775-2785, 2013.

[11] X. Zhang, "Reversible Data Hiding With Optimal Value Transfer", *IEEE Trans. on Multimedia.*, vol. 15, no. 2, pp. 316-325, 2013.

[12] B. Ou, X. Li, Y. Zhao, R. Ni and Y. Shi, "Pairwise prediction-error expansion for efficient reversible data hiding", *IEEE Trans. on Image Process.*, vol. 22, no.12, pp. 5010 - 5021, 2013.